Cooperativity in Surface Bonding and Hydrogen Bonding of Water and Hydroxyl at Metal Surfaces

ARTICLE *in* THE JOURNAL OF PHYSICAL CHEMISTRY C · JUNE 2010

Impact Factor: 4.77 · DOI: 10.1021/jp101855v

Structure and Bonding of the Water−Hydroxyl Mixed Phase on Pt(111)

T. Schiros,[†,‡] L.-Å. Näslund,[†,‡] K. Andersson,[†,‡] J. Gyllenpalm,[†,‡] G. S. Karlberg,[§] M. Odelius,[†] H. Ogasawara,[‡] L. G. M. Pettersson,[†] and A. Nilsson*[,†,‡]

Department of Physics, Stockholm University, AlbaNova University Centre, SE-106 91 Stockholm, Sweden, Stanford Synchrotron Radiation Laboratory, P.O. Box 20450, Stanford, California 94309, and Department of Applied Physics, Chalmers/Göteborg University, S-41296 Göteborg, Sweden

Received: May 3, 2007; In Final Form: July 20, 2007

We combine low-energy electron diffraction (LEED), X-ray photoelectron spectroscopy (XPS), X-ray absorption spectroscopy (XAS), and Auger electron spectroscopy (AES) with density functional theory (DFT) to reveal the structure and bonding of water−hydroxyl mixed layers adsorbed on Pt(111). We find that the stable water−hydroxyl adlayer forms a mixed phase of nearly coplanar hexamer structures resulting in $(\sqrt{3} \times \sqrt{3})R30°$ and (3×3) unit cells, respectively. In the asymmetric (3×3) structure the lateral O−O distances alternate between long and short bond lengths similar to the chemical bonding network for OH^- ions in solution. The chemical driving force behind this similarity is discussed in a molecular orbital picture.

1. Introduction

Hydroxyl (OH) species play an important role in many surface chemical processes in humid environment where these OH species are surrounded by coadsorbed water molecules (H_2O). As such, knowledge of the site occupation and orientation of the adsorbed OH species, as well as of the surrounding H_2O, is a fundamental prerequisite to understanding the chemical properties of model reaction intermediates such as the H_2O + OH mixed layer. Furthermore, OH is considered an essential reaction intermediate in both hydrogen production and fuel cell electrocatalysis where platinum (Pt) has been identified as the most active metal.

Despite the intense interest, the structure and bonding of the OH species on hexagonal metal surfaces, e.g., Pt(111), and its interaction with surrounding water are still subjects of debate. Theoretical work by Michaelides and Hu[1,2] indicates that at higher coverages OH preferentially occupies top sites and decomposes via the reversible reaction $2OH(a) \rightarrow O(a) + H_2O(a)$ with a low activation barrier unless stabilized by surrounding water. Various experimental studies, e.g., temperature-programmed desorption (TPD), low-energy electron diffraction (LEED), and scanning tunneling microscopy (STM) have confirmed that OH occupies top sites, is stabilized by a H-bonding network, and forms a $(\sqrt{3} \times \sqrt{3})R30°$ periodicity.[3−5] Further, the studies report that the $(\sqrt{3} \times \sqrt{3})R30°$ phase coexists with a (3×3) phase and that each of these phases has a coverage of 0.67 ML in their most stable conditions. The coverage of the H_2O + OH mixed phase has also been suggested to be as high as 0.75 ML due to a 2:1 $H_2O(a)$ + O(a) reaction stoichiometry as proposed by Creighton and White[6] and Bange et al.[7] Their results indicate that two water molecules per atomic oxygen are necessary to obtain a stable phase of H_2O + OH on the Pt(111) surface. Since atomic oxygen forms a (2×2) structure on Pt(111)[8−10] with a coverage of 0.25 ML,[10−12] complete conversion of O(a) into OH(a) through coadsorption of two $H_2O(a)$ for each preadsorbed O would result in a total coverage of 0.75 ML. TPD studies give similar, although slightly higher, total coverage values, which shows that a saturated O precoverage gives ∼0.84 ML of H_2O + OH mixed layer corresponding to 2.3 H_2O for each preadsorbed O.[4] The H_2O + OH mixed layer obtained from 0.25 ML O precoverage is, however, less stable than that generated from lower O coverages, e.g., 0.15 ML preadsorbed O. In either case, both the OH groups and the stabilizing water molecules are more strongly bonded to the Pt surface than pure water on Pt(111). This is reflected in TPD studies which show a higher desorption temperature for water in the H_2O + OH mixed phase on Pt(111) than for the corresponding pure water monolayer.[4,13,14]

The H_2O + OH mixed monolayer has been suggested to form a nearly flat layer with no internal O−H bonds perpendicular to the Pt surface.[15] This picture, which is supported by a recent infrared (IR) spectroscopy study,[4] implies that the molecular axis of the OH is parallel to the Pt surface and that the stabilizing water molecules lie flat and bond to Pt through the oxygen. Further theoretical works support this configuration for H_2O and OH and also indicate top site occupation for both adsorbates with only a small tilt of the molecular axis of OH relative to the surface plane.[1,2,15−18] In addition, geometry optimization predicts that the observed (3×3) structure is a H_2O + OH phase with asymmetric O−O distances; the OH accepting H-bonds from H_2O are short and the OH donating H-bonds toward H_2O are long.[15] This contradicts the asymmetry suggested in a LEED study by Held et al.,[19] where the authors found twice as many long bonds as short ones and attributed the short bonds to OH donating H-bonds to H_2O. Thus, the OH−water interaction on Pt(111) remains an open question.

As the structure of the adsorbate layer and local interactions to a large extent determine reactivity, it is important to establish both. Recently the combination of core-electron spectroscopies, including X-ray photoelectron spectroscopy (XPS), X-ray absorption spectroscopy (XAS), and X-ray emission spectroscopy (XES), proved to be particularly useful in elucidating the local structural properties and interactions in the first water

* Corresponding author. Tel.: +1 (650) 926 2233. Fax: +1 (650) 926 4100. E-mail: nilsson@slac.stanford.edu.
[†] Stockholm University.
[‡] Stanford Synchrotron Radiation Laboratory.
[§] Chalmers/Göteborg University.

10.1021/jp073405f CCC: $37.00
Published on Web 09/22/2007

adlayer on Pt(111).[20] Extraction of such information is facilitated by the localization of the core hole and the dependence of the core-level binding energy of a particular element on its chemical environment. In this way, XPS and XAS provide element-specific probes of the local and chemical surroundings of a given adsorption site.[21] In particular, XAS is sensitive to the local configuration and bond length of the donating H-bond in the H-bonded network of water molecules.[20,22−25] Moreover, by fine-tuning the core-excitation energy to different XAS resonances it is possible to distinguish different adsorbed species by Auger electron spectroscopy (AES).[21,26,27] With the use of these techniques, the molecularly intact water monolayer adsorbed on Pt(111) was shown to form a nearly flat layer (0.25 Å O−O corrugation) with alternating metal−oxygen (M−O) and metal−hydrogen (M−HO) bonds.[20]

In the present work, we use the insights gained from the water on Pt(111) system and extend our investigation to address the H-bonding structure and interactions in a D_2O + OD mixed layer on Pt(111) formed by D_2O + O surface chemistry. We combine LEED, XPS, XAS, and AES with density functional theory (DFT) based structure calculations and XPS and XAS spectrum calculations. The combination of experiment and theory makes it possible to derive a detailed picture of the molecular orientation and nature of the chemical bonding of adsorbates on well-defined single-crystal surfaces.[20,28,29]

2. Experimental Methods

The experiment was performed at the elliptically polarized undulator (EPU) beamline 11.0.2 at the Advanced Light Source (ALS), the synchrotron light facility operated by Lawrence Berkeley National Laboratory and at the EPU beamline 5-1 at the Stanford Synchrotron Radiation Laboratory (SSRL) in California. The XPS and AES spectra were obtained using a Scienta SES-100 electron energy analyzer,[30] and the partial electron yield (PEY) XAS spectra were obtained through a multichannel plate (MCP) device[31] where the retardation voltage was −320 V. The total energy resolutions were better than 0.1 eV in all used spectroscopy techniques. The LEED patterns were obtained using a retarding field analyzer (ErLEED 100, SPECS).[32]

The sample was continuously cooled with liquid nitrogen (LN_2), and the temperature, in the interval of <100 to 250 K, was controlled by IR radiation from a 0.15 mm thoriated-tungsten filament. (W99/Th1)[33] mounted ca. 2 mm from the backside of the Pt crystal. The temperature was monitored using an alumel/chromel thermocouple spot-welded via a small piece of tantalum foil on the side of the Pt crystal and calibrated against the desorption onset of a D_2O multilayer, reported to be 140 K,[13,34] to ensure that no small offsets occurred.

The Pt(111) crystal was cleaned by several sputter−anneal cycles. Sputtering was performed with neon ion bombardments for 3 min at a sputter current (I_{Ne}) = 5 μA/cm^2, and annealing temperatures were ∼950 K. During cool-down, in the temperature interval of 800−400 K, the Pt surface was treated with O_2. Surface order and cleanliness was confirmed through observation of a sharp (1 × 1)-Pt(111) LEED pattern and the absence of O1s and C1s photoelectron peaks, confirming contamination levels below 0.1% of a monolayer.

The coadsorbed monolayer was prepared following the procedure from ref 14. A (2 × 2)-O layer was prepared at T < 100 K by an O_2 dose until saturation and thereafter heated to 350 K.[35] Water, in the form of D_2O, was supplied at T < 100 K until a multilayer was achieved. Subsequent heating to 156 K, with a heat ramp of ∼0.5 K/s and 10 s delay time before cool-down, desorbed weakly bonded D_2O molecules as confirmed by the chemical shift of the O1s photoelectron peak between the multilayer adsorbed D_2O and the D_2O/Pt(111) adsorbed water molecules.[36] This process produced a stable D_2O + OD layer. Coverages were calibrated against 0.5 ML CO/Pt(111), which at <100 K adsorbs nondissociatively in a 1:1 ratio between top and bridge sites.[12,37]

XPS, XAS, and AES were performed in ultrahigh vacuum (UHV) conditions with a base pressure better than 3 × 10^{-11} torr. These conditions limited the surface contamination to negligible levels, routinely confirmed with C1s XPS before and after each series of spectra recordings. The XAS spectra were recorded with the photon **E**-vector perpendicular and parallel to the surface, referred to in the text as out-of-plane and in-plane geometry, respectively. The change in orientation of the **E**-vector was obtained using the beamline EPU. In XPS and AES, the Pt surface was perpendicular to the lens axis of the Scienta electron energy analyzer. AES spectra were recorded in Auger geometry with the photon **E**-vector perpendicular to the lens axis of the Scienta electron energy analyzer, i.e., parallel to the Pt surface, to minimize the photoemission background. XPS, on the other hand, was performed in photoemission geometry with the photon **E**-vector parallel to the lens axis. In all measurements a grazing incident angle of the photon beam to the sample of 4° was used, which gave an illuminated area of 100 × 1400 μm^2 on the sample surface.

To avoid radiation-induced dissociation and desorption the samples were scanned with speeds >15 μm/s. Furthermore, by using soft X-ray photons, which have a higher absorption cross section for creation of core holes than, e.g., an electron beam, we minimize damage to our sample from the incident radiation during the detection of Auger electrons generated from the core hole decay. Without these precautions damage to the samples was observed and identified.

3. Theoretical Methods

3.1. Geometry. To interpret the data from the experimental measurements a geometrical model for the adsorbates on the surface is needed. To this end we introduce four geometrical models, labeled A−D, which together span most of the structures suggested in the literature for H_2O + OH coadsorbed on Pt(111). All four models are shown in Figure 1 with O−O distances given in Table 1.

Models A and B correspond to the most stable H_2O + OH structures of $(\sqrt{3} \times \sqrt{3})R30°$ and (3 × 3) symmetry as given by first-principles DFT calculations based on the Perdew−Wang 91 (PW91) functional[38] for the exchange and correlation. The details of these calculations have been published previously.[15] Both structures are characterized by long OH donating H-bonds and short OH accepting H-bonds, which is similar to the O−O bond length asymmetry found for OH^- ions in solution.[39]

Models C and D represent other geometric structures put forward in the literature, as will be described below. Since these models are not predicted by DFT we obtain them by modifying the appropriate bond distances in model A. For model C we replaced the alternating O−O distances of model A with a constant O−O separation of 2.77 Å to represent a symmetric $(\sqrt{3} \times \sqrt{3})R30°$ phase often assumed in previous studies, for example, see refs 14, 18, and 19. Model D represents a geometrical model proposed by Held et al.[19] with long OH accepting and short donating H-bonds (opposite asymmetry compared to model A). We constructed model D from model A by modifying the relevant O−O distances to reproduce the

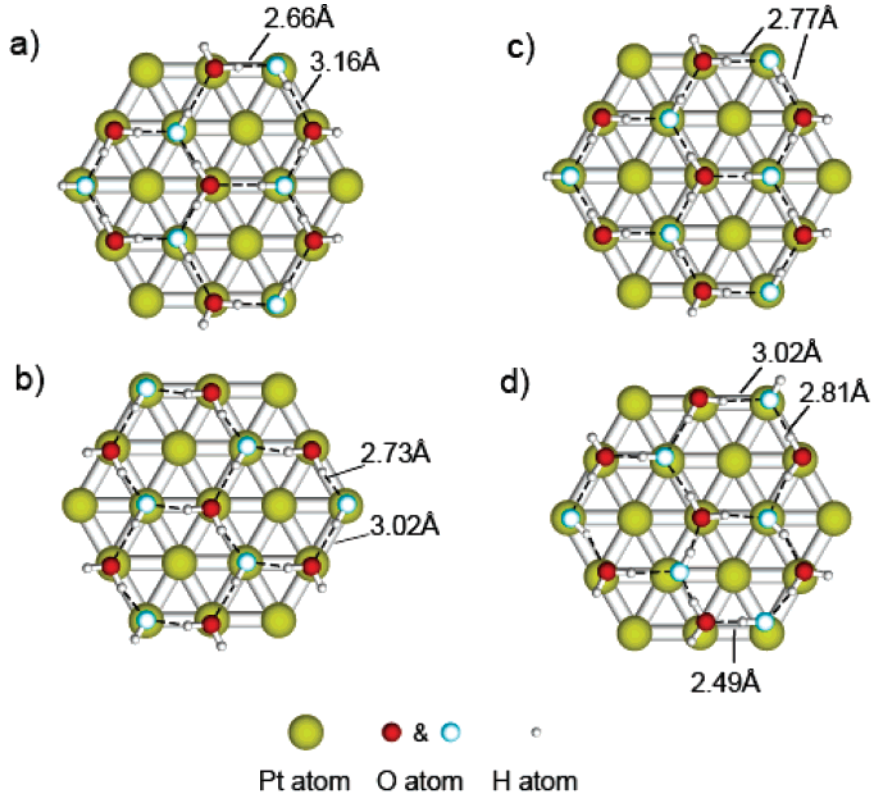

Figure 1. Four structure models of H_2O + OH coadsorbed on Pt(111): (a) asymmetric (3 × 3) phase with long OH donating H-bond and short OH accepting H-bonds, R(O−O) = 3.16 and 2.66 Å, respectively, (b) asymmetric ($\sqrt{3} \times \sqrt{3}$)$R30°$ phase with long OH donating H-bond and short OH accepting H-bonds, R(O−O) = 3.02 and 2.73 Å, respectively, (c) symmetric ($\sqrt{3} \times \sqrt{3}$)$R30°$ phase, R(O−O) = 2.77 Å, and (d) asymmetric (3 × 3) with short OH donating and long OH accepting H-bonds, R(O−O) = 2.49 and 2.81 or 3.02 Å. Oxygen atoms that belong to water are dark (the oxygen atoms are red on water and blue on hydroxyl). The figure shows only the first Pt layer, although three to five layers were used in the DFT calculations. The Pt layers and all adsorbed molecules were allowed to relax resulting in a 0.05−0.14 Å buckling of the first Pt layer. The surface relaxation, furthermore, resulted in H_2O−Pt and HO−Pt distances in the range of 2.1−2.2 and 2.0−2.1 Å, respectively.

TABLE 1: O−O Distances in the Four Considered Structure Models of H_2O and OH Coadsorbed on Pt(111)[a]

model	phase	R(O−O) OH accepting H-bond [Å]	R(O−O) OH donating H-bond [Å]
A	(3 × 3)	2.66	3.16
B	($\sqrt{3} \times \sqrt{3}$)$R30°$	2.73	3.02
C	($\sqrt{3} \times \sqrt{3}$)$R30°$	2.77	2.77
D	(3 × 3)	2.81 or 3.02	2.49

[a] Models A and B are obtained from our first-principles DFT calculations, whereas models C and D represent structures suggested or assumed in the literature; model C is from refs 14, 18, and 19, and model D is from ref 19.

local H-bond geometries around OH and H_2O in the structure derived from LEED.[19] In all four models the DFT optimized Pt slab of model A is employed. Hence, the models only differ in the lateral O−O distances and subsequent distortions of the H-bond network.

In model B the HO−Pt and H_2O−Pt distances vary between 2.0 and 2.1 Å and 2.1 and 2.2 Å, respectively, whereas for the other models these distances are 2.1 and 2.2 Å, respectively, with very little deviation. Hence, in all four models the coadsorbed layer is nearly coplanar. To obtain the distance dependence of the XAS peaks we systematically varied the HO−Pt and H_2O−Pt distances and computed XAS spectra. The out-of-plane XAS spectrum computed for the O−Pt distance predicted by the first-principles DFT calculations most closely resembles the experimentally recorded spectrum, confirming the accuracy of the optimization. In all cases except model B the Pt−O−H angle is larger for OH than for H_2O: 108.9° compared to 97.9°. In model B the Pt−O−H angles for OH (102.9°) and H_2O (100.3°) are quite similar. This, in conjunction with the overlap in the range of O−Pt distances for OH and H_2O, results in an essentially flat adlayer in model B. The computed buckling of the first Pt layer due to surface relaxation and interaction with the H_2O + OH layer ranges from 0.05 to 0.14 Å which is in excellent agreement with the values obtained from LEED.[19]

Other models, which include Pt−HO bonds, dangling H-bonds perpendicular to the surface, and more corrugated layers, have also been considered. They were, however, rejected at an early stage of the study due to poor agreement between DFT calculated XPS and XAS spectra and experiment.

3.2. Spectra Calculations. In order to compute XAS and XPS spectra the periodic structures were reduced to cluster models consisting of 37 Pt atoms in three layers with 19 Pt atoms in the first layer, 12 in the second, and 6 in the third. The adsorbed layer included 13 oxygen atoms and 21 or 20 hydrogen atoms depending on whether the core-excited O belonged to H_2O or OH. The Pt atoms were described using a double-ζ plus polarization basis set in combination with a 16-electron relativistic effective core potential (ECP) developed by Wahlgren.[40] The oxygen and hydrogen atoms were described using triple-ζ plus polarization basis sets. Hydrogen has the (5s) basis of Huzinaga[41] contracted to 3s and with one p-function added. The core-excited (in the case of XAS) and the core-ionized (in the case of XPS) oxygen was described using the IGLO-III all-electron basis set of Kutzelnigg et al.[42] All other oxygen atoms were described using ECP,[43] which eliminates the O1s level in order to simplify the definition of the core hole.

Calculations of XAS, XPS, and XES spectra were performed with gradient-corrected DFT using the StoBe-deMon code.[44] In all calculated X-ray spectra the exchange-correlation contributions were estimated using gradient-corrected exchange and correlation functionals of Becke,[45] and Perdew.[46] XAS spectra were generated within the transition potential approach of Triguero et al.,[47] where the core and valence relaxation is modeled by half a core hole on the atom. In the spectrum calculation the normal molecular basis set is augmented by a large diffuse basis (~150 functions) to improve the description of the Rydberg and continuum states.[48]

The XAS spectra were computed in the dipole approximation where the intensity is given by the dipole transition matrix elements. An XAS spectrum calculation thus results in a discrete set of energy levels, each with associated oscillator strength and line broadening. The experimental broadening of a transition depends on instrumental, lifetime, and vibrational effects, which can be simulated by convoluting the obtained oscillator strengths in the theoretical spectra with Gaussians of linearly increasing full width at half-maximum (fwhm). For comparison with experiment, the XAS oscillator strengths were thus broadened with a constant value of 0.7 eV below the ionization potential and a linearly increasing value up to 8 eV over a 10 eV interval above it, after which the width was kept constant.[23,24] The half-core hole approach accounts for relaxation up to second order and reproduces the core-level excitation energy to within 2 eV of the experimental value. The final XAS energy scale for the theoretical spectra was corrected for relaxation effects through the ΔKohn−Sham approximation of Kolczewski et al.[49] and for the relativistic O 1s shift of +0.33 eV.[50] Finally, all computed XAS spectra were systematically shifted +0.17 eV to agree with the 540 eV resonance in the in-plane spectrum, which is the spectral "fingerprint" of the intermolecular H-bond network.[22,23,25,51]

XPS binding energies were likewise computed in the ΔKohn−Sham approach,[52] i.e., relative the ionization potential, and then shifted by 5.16 eV to compensate for the work function of the system. Broadening of the computed XPS was based on the line shape of the recorded XPS of O/Pt(111) and D_2O/Pt(111) with the constraint of a 1:1 H_2O/OH ratio.

The XES spectra were computed within the dipole approximation of the transition between the O 1s core hole and the occupied valence states, from the ground state electronic structure, which gives the best representation of the spectrum.[53] The highest occupied molecular orbital in the cluster calculations was taken as Fermi level for the XES binding energy scale. The computed oscillator strengths were convoluted with 1.0 eV Gaussians.

4. Results and Discussion

4.1. Low-Energy Electron Diffraction. LEED patterns are invaluable in identifying the phase of the water−hydroxyl adlayer in the corresponding XPS, XAS, and AES experiments. LEED, measured with electrons with kinetic energy (E_k) = 46 eV, indicates the coexistence of two coadsorbed structures. A bright pattern has been identified as the $(\sqrt{3} \times \sqrt{3})R30°$ structure, whereas weak but sharp spots between the $(\sqrt{3} \times \sqrt{3})R30°$ spots correspond to the (3 × 3) phase. This mixed phase of (3 × 3) and $(\sqrt{3} \times \sqrt{3})R30°$ structures is stable over a range of temperatures and D_2O/OD ratios, but at very high (>1) and very low (<1) D_2O/OD ratios, the (3 × 3) pattern disappears and only the $(\sqrt{3} \times \sqrt{3})R30°$ structure is observed. This trend was also reported by Clay et al.[4] and Held et al.[19] who observed the $(\sqrt{3} \times \sqrt{3})R30°$ and (3 × 3) mixed phase as the H_2O/OH ratio approached unity and the intermolecular H-bonded network was completed but only the $(\sqrt{3} \times \sqrt{3})R30°$ structure at other stoichiometric ratios. However, LEED alone is not enough to eliminate the possibility of a mixed $(\sqrt{3} \times \sqrt{3})R30°$ and (3 × 3) adlayer for D_2O/OD ratios far from unity, in fact, such a layer has been observed with STM without a corresponding (3 × 3) LEED pattern.[3,5] In such cases, the size of the (3 × 3) domains is simply too small to generate an observable LEED pattern.

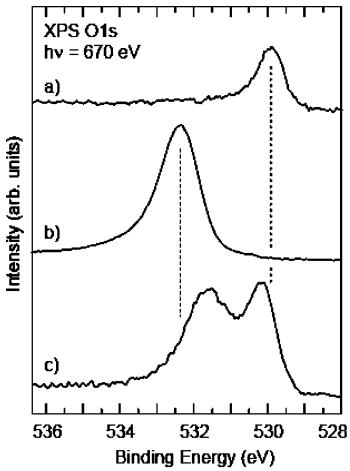

Figure 2. Experimental O 1s XPS for (a) atomic O/Pt(111), (b) D_2O/Pt(111), and (c) (D_2O + OD)/Pt(111). The excitation energy was 670 eV, and to avoid beam damage, the spectra were recorded while scanning the sample at 35 μm/s.

4.2. X-ray Photoelectron Spectroscopy. By comparing O 1s XPS of O/Pt(111), D_2O/Pt(111), and (D_2O + OD)/Pt(111), as shown in Figure 2, we can readily observe changes in the chemical environment of oxygen in the different systems. The O 1s photoelectron peak for O/Pt(111) is located at a binding energy (E_{BE}) of 529.9 eV and corresponds to 0.25 ML coverage. Comparison with an earlier XPS study of different adsorption phases of oxygen on Pt(111)[54] confirms that the recorded spectrum in Figure 2a reflects atomic oxygen adsorbed in hollow sites in a (2 × 2)-O overlayer.[10,11] The O 1s photoelectron peak for D_2O/Pt(111) is located at E_{BE} 532.3 eV and corresponds to 0.7 ML coverage.[20] The broad XPS feature of D_2O/Pt(111) has been interpreted in terms of two peaks reflecting the alternating Pt−O and Pt−HO bonds in a nearly flat H-bonded network on Pt(111) with three H-bonds per water molecule.[20] The XPS spectrum of (D_2O + OD)/Pt(111) shows two peaks located at 530.1 and 531.6 eV, which we attribute to OD and D_2O species, respectively. The three spectra in Figure 2 clearly show chemical shifts between the coadsorbed layer on Pt(111) compared to pure atomic oxygen on Pt(111) and pure water on Pt(111), respectively. This indicates that all oxygen atoms are in different chemical environments in the D_2O + OD mixed layer compared to the corresponding pure systems and, furthermore, that the majority of preadsorbed oxygen atoms are involved in the OD formation. XAS results, discussed in section 4.4, further indicate that no atomic oxygen remains in the D_2O + OD mixed phase.

It is possible to estimate the amount of uncoordinated surface Pt atoms in the sample by comparing the Pt 4f XPS spectra for clean Pt(111) with that for the coadsorbed layer of (D_2O + OD)/Pt(111).[12,20] The Pt $4f_{7/2}$ XPS spectrum of the clean Pt(111) surface is presented in Figure 3a and shows two peaks at E_{BE} of 70.6 and 70.9 eV, respectively. The low-energy peak originates from surface Pt atoms exposed to vacuum, whereas the high-energy peak originates from bulk Pt atoms. Figure 3b shows Pt $4f_{7/2}$ XPS of a Pt surface covered with the D_2O +

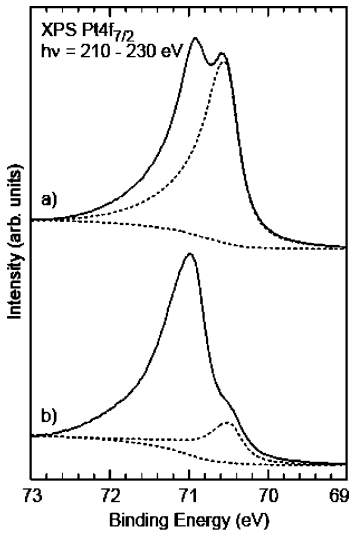

Figure 3. Experimental Pt $4f_{7/2}$ XPS for (a) clean Pt(111) and (b) (D_2O + OD)/Pt(111). Out of consideration for photoelectron diffraction effects the spectra were recorded at three excitation energies, 210, 220, and 230 eV, and thereafter summed. To avoid beam damage the spectra were recorded while scanning the sample at 35 μm/s. The dotted peaks, which represent the contribution from uncoordinated Pt atoms at the surface, were obtained from a curve fitting analysis.

OD coadsorbed phase obtained from a saturated (2 × 2)-O coverage. The intensity due to uncoordinated surface Pt atoms decreases by 80%, and the coordinated surface Pt atoms show a chemical shift to a higher E_{BE} peak at 71.0 eV, which also includes the bulk Pt contribution. Thus, the amount of uncoordinated surface Pt atoms in (D_2O + OD)/Pt(111) obtained from a saturated (2 × 2)-O coverage corresponds to 0.2 ML. Any relevant structural model must therefore accommodate a percentage of uncoordinated Pt atoms.

4.3. Temperature-Dependent X-ray Photoelectron Spectroscopy. The reaction between adsorbed water and oxygen to form OD(a) does not proceed spontaneously on Pt(111) at temperatures <100 K. A temperature increase, from <100 to ~155 K, is needed to promote hydroxyl formation.[14] Figure 4 shows a series of O 1s XPS spectra where the temperature is increased by ~5 K (heat rate ~0.5 K/s) between each recorded spectrum. The top panel shows intensity versus E_{BE} where the spectrum at the lowest temperature (120 K), corresponding to multilayer D_2O, is in the background. In the bottom panel, which shows temperature versus E_{BE} and color-coded intensity, the topmost spectrum corresponds to multilayer D_2O. At 140 K, D_2O in the multilayer starts to desorb and the peak intensity decreases. Further temperature increase shifts the D_2O peak from 532.7 to 531.6 eV until the temperature reaches 166 K. In this temperature range the low E_{BE} peak, which at 120 K corresponds to the precovered (2 × 2)-O, shifts from 529.9 to 530.1 eV and increases in intensity (not visible in the top panel). The chemical shifts indicate that hydroxyl formation appears in the temperature interval of 130−166 K. Further, the temperature-dependent XPS also shows that OD coexists with D_2O and that the water−hydroxyl phase is stable over a 30 K temperature range (~155−185 K) before water starts to desorb. At ~185−190 K a reversible process is observed, which includes OD dissociation and D_2O formation according to $2OD(a) \rightarrow O(a) + D_2O(a)$[1,2] followed by an immediate D_2O desorption leaving behind atomic oxygen, see the lower panel of Figure 4. On the other hand, if the heat increase stops within the temperature range of 130−185 K, i.e., when the water−hydroxyl mixed phase is formed, and the sample is cooled back to temperatures <130 K the formed D_2O + OD layer remains stable.

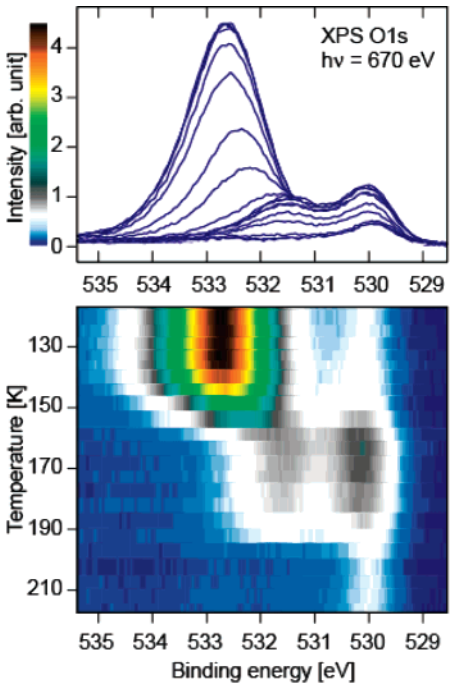

Figure 4. Temperature-dependent O 1s XPS for D_2O and OD coadsorbed on Pt(111). The spectra were recorded in the range of 120−215 K with ~5 K interval (heat rate ~0.5 K/s). The spectrum recorded at the lowest temperature (120 K), corresponding to multilayer D_2O and atomic O(a) (contribution from O(a) is not visible in the top panel), is shown in the background (top panel) and as the topmost spectrum (bottom panel), respectively. The excitation energy was 670 eV.

4.4. X-ray Absorption Spectroscopy. XAS offers complementary information related to the structure of the coadsorbed layer.[21,31] The resonance intensity associated with a particular final state in XAS is largest if the **E**-vector of the incoming light points in the same direction as the p-component in the final state orbital on the excited atom and vanishes if the **E**-vector is perpendicular to this direction. Hence, by using linearly polarized synchrotron radiation, information about the structure formed by the adsorbed molecules can be obtained via angle-resolved measurements. A strong polarization dependence of the XAS spectra indicates a well-defined adsorption geometry for the system.

The O 1s XAS for O/Pt(111), D_2O/Pt(111), and (D_2O + OD)/Pt(111) prepared under the conditions described above is shown in Figure 5. The left panel shows spectra recorded in the in-plane geometry (**E**-vector parallel to the surface), and the right panel shows spectra recorded in the out-of-plane geometry (**E**-vector perpendicular to the surface). The strong peak at ~531 eV in the O/Pt(111) in-plane spectrum (Figure 5a, left panel) corresponds to atomic oxygen on the Pt surface. This peak is absent in Figure 5c, left panel, indicating that no atomic O is present on the Pt surface in the D_2O + OD mixed phase. With this we confirm that all preadsorbed atomic oxygen has been involved in the hydroxyl formation and construction of the D_2O + OD mixed phase. The XAS spectrum of the coadsorbed phase (Figure 5c, left panel) is instead dominated by a resonance at 540 eV which is the signature of the in-plane H-bond network similar to pure water on Pt(111) shown in Figure 5b, left panel. The dominance of the high-energy structure at 540 eV and lack of comparable preedge spectral feature due to uncoordinated O−D groups at 535 eV[22,23,51] indicate that all H-bonds in the plane are saturated.[22,23,51] This implies that the origin of the

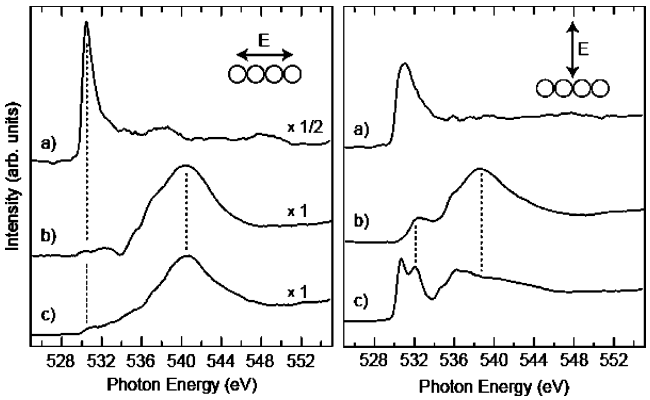

Figure 5. Experimental O 1s XAS spectra of (a) atomic O/Pt(111), (b) D_2O/Pt(111), and (c) (D_2O + OD)/Pt(111). The spectra were recorded with the photon **E**-vector parallel (left panel) and perpendicular (right panel) to the surface. Note that the atomic O/Pt(111) XAS spectrum in the left panel is scaled by a factor 0.5. To avoid beam damage the spectra were recorded while scanning the sample at 20 μm/s.

XPS peak at 530.1 eV (Figure 2c) can only be hydroxyl species stabilized by surrounding H-bonded water in a saturated H-bond network.

The corresponding out-of-plane XAS spectra are given in the right panel of Figure 5. All three spectra, the D_2O + OD coadsorbed phase in particular, show **E**-vector polarization dependence (compare left and right panels). Unlike the in-plane spectrum, the out-of-plane spectrum of (D_2O + OD)/Pt(111) is dominated by structures in the low-energy region. Furthermore, in contrast to the rather similar in-plane spectra (Figure 5, left panel), the out-of-plane spectra of D_2O/Pt(111) and (D_2O + OD)/Pt(111) are completely different from one another. The out-of-plane spectrum of D_2O/Pt(111) (Figure 5b, right panel) is dominated by intensity around 538.5 eV, which is absent in the XAS spectrum of (D_2O + OD)/Pt(111) (Figure 5c, right panel). As this resonance is related to metal−hydrogen (M−HO) bonds,[20] the comparison reveals that no such bonds exist in the water−hydroxyl layer on the Pt surface. Thus, in the D_2O + OD mixed layer D_2O bonds to the Pt surface solely through its oxygen. Earlier IR studies observe no O−D stretch in the D_2O + OD mixed phase on Pt(111),[4] supporting the view that all internal O−D groups in OD and water are near parallel with the Pt surface.

The low-energy structure in the out-of-plane spectrum of (D_2O + OD)/Pt(111) is dominated by two sharp peaks (Figure 5c, right panel). The first peak at 530.7 eV is much sharper than the XAS peak of O/Pt(111) (Figure 5a, right panel) and has no analogue in the spectrum for D_2O/Pt(111) (Figure 5b, right panel). This peak is related to depopulation of the oxygen lone pair (O lp) of hydroxyl into the Pt substrate to minimize Pauli repulsion and facilitate bonding. The second peak at 532.1 eV coincides in energy with the depopulation of the water O lp into the Pt(111) d-states.[20]

For a monolayer of pure water adsorbed on a close-packed metal surface the ratio between water molecules with both O−H bonds parallel to the surface (often called the O-bonding channel) and water molecules with one O−H bond parallel and one O−H perpendicular to the surface (either H-up or H-down) is 1:1.[20,29,56] The O-bonding channel is the dominant bonding mechanism for water on metal surfaces,[55] and further interaction between the water layer and the substrate results from a balance between the strength of bonding to the surface and the intermolecular H-bond network. As a result, some metal surfaces, e.g., Pt(111) and Ru(001), find it favorable to have

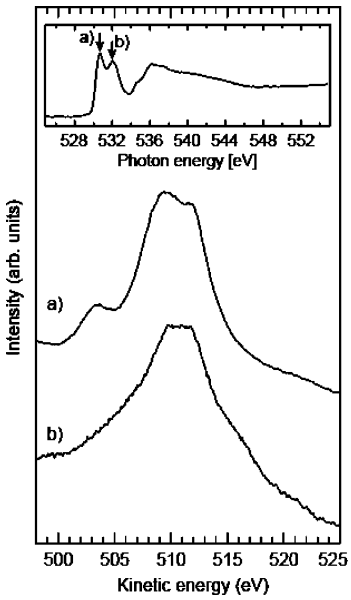

Figure 6. Auger electron spectroscopy (AES) spectra recorded at (a) 530.7 and (b) 532.1 eV, i.e., at energies that correspond to the first and second peak in the out-of-plane O 1s XAS spectrum (see inset). The photoemission signal from the substrate has been subtracted.

water molecules that point one hydrogen down toward the surface,[20,56,57] whereas other metal surfaces, e.g., Cu(110) and Rh(111), have water molecules that also point one hydrogen away from the surface.[29,58] In the case of the H_2O + OH mixed phase on Pt(111), which has 25% fewer H-bonds than the corresponding case of pure water, the combination of the dominant O-bonding channel and the stability in a complete in-plane intermolecular H-bond network requires that both water and hydroxyl donate all their H-bonds to each other. Hence, an H_2O + OH mixed phase with $(\sqrt{3} \times \sqrt{3})R30°$ or (3×3) symmetry needs to have all internal O−H bonds parallel to the surface. Accordingly, models considered with Pt−HO bonds or OH directed toward the vacuum were unable to reproduce the experimental data. Isolated OH, on the other hand, is predicted to adsorb upright on close-packed surfaces.[59,60]

4.5. Auger Electron Spectroscopy. To verify the chemical origin of the two peaks in the out-of-plane O 1s XAS spectrum we have used AES with selective excitation energies.[21,26,27] For molecules with a strong electronic interaction with the substrate, the electron excited in the X-ray absorption process delocalizes on a time scale shorter than that of the core hole decay process.[21,27] In this sense the AES spectra are independent of the excitation energy. However, variation in the AES spectra as a function of excitation energy can in fact be observed if the X-ray absorption, as identified through various XAS spectral features, is related to different surface species, which further produce different AES lines. This was first demonstrated in the case of N_2 on Ni(100) where the AES spectra of the two inequivalent nitrogen atoms could be distinguished using selective excitation.[26]

Figure 6 presents two AES spectra recorded at excitation energies that coincide with the first two structures from the out-of-plane XAS spectrum corresponding to 530.7 and 532.1 eV (see inset in Figure 6). The AES spectrum obtained at 530.7 eV excitation energy shows a significantly different spectral shape compared to the AES spectrum obtained at 532.1 eV. For instance, the latter spectrum is considerably broadened with respect to the former, particularly around 505 eV kinetic energy. The difference in Auger electron signature at the two O 1s XAS resonances can be attributed to different chemical species.[21,26,27]

This observation suggests that the first peak originates from only one type of species, which can only be hydroxyl based on that the O1s binding energy in D_2O is too high, whereas the second peak originates from all different oxygen containing species, i.e., both water and hydroxyl, on the Pt surface.

4.6. Evaluation of Different Models with Respect to the Experimental Results. All models considered are constrained by the experimental results mentioned above. The first-principles DFT calculations, for example, generate (3 × 3) and ($\sqrt{3}$ × $\sqrt{3}$)*R*30° structures that both fulfill the conditions of a saturated H-bonding network parallel to the surface with no internal O−H bond perpendicular to the surface while containing uncoordinated Pt atoms (see Figure 1). The asymmetry of both the (3 × 3) and ($\sqrt{3}$ × $\sqrt{3}$)*R*30° structures obtained from the DFT calculations rests in a lateral displacement of the O atoms from top sites resulting in a lengthening or shortening of the donating H-bond to either hydroxyl or water. The nature of the asymmetry (long OH donating H-bond/short OH accepting H-bond or vice versa) is an issue of controversy. For instance, Held et al.[19] interpreted their data as evidence for twice as many long O−O separations (2.81 or 3.02 Å) as short O−O distances (2.49 Å) in the (3 × 3) phase. The authors speculated that the short O−O distance belongs to OH donating a H-bond to H_2O and attributed the longer distances to OH accepting H-bonds. This assignment is opposite to what one may expect from the bonding of OH^- ions in solution,[39] where the OH^- donating H-bond is very long (~3.5 Å) and the OH^- accepting H-bond is quite short (~2.3 Å), as well as to our first-principles DFT calculations which instead predict long OH donating H-bonds and short OH accepting H-bonds.

Since XAS is sensitive to the local environment of the H-bond network, including the length and directionality of chemical bonds,[20,22,23,25,61] the technique can distinguish between the different postulated structures and therefore directly suggest exclusion, refinement, or acceptance of a particular model. The ability to reliably generate spectra for different types of core-excited oxygen atoms (belonging to OH or H_2O in a range of adsorption geometries) allows for a theoretical decomposition of the recorded XAS spectrum and positive assignment of the different spectral features.

We thus turn our attention to the details of the four different structural models (Figure 1 and Table 1) and the corresponding calculated out-of-plane XAS spectra for each, as shown in Figure 7. Figure 1 summarizes the models: model A with long OH donating (*R*(O−O) = 3.16 Å) and short OH accepting (*R*(O−O) = 2.66 Å) H-bonds; model B with OH donating and OH accepting H-bonds with O−O distances of 3.02 and 2.73 Å, respectively; model C characterized by an O−O distance of 2.77 Å between all species; and model D which considers the structure proposed by Held et al.,[19] with short OH donating (*R*(O−O) = 2.49 Å) and long OH accepting (*R*(O−O) = 2.81 or 3.02 Å). For all four models the computed XAS spectrum produces two sharp peaks around 530 and 532 eV, corresponding to depopulation of charge into the Pt substrate from the O lone pair of OH and H_2O. For models A and B, but not for models C and D, the second peak (532 eV) includes contributions from both OH and H_2O. The fact that the second peak in models C and D does not overlap with H_2O contributions and is therefore due to OH transitions alone disagrees with the AES data, which directly shows that resonances from both hydroxyl and water contribute to this peak. It is not, however, necessary for the individual constituents of a mixed phase system (here the ($\sqrt{3}$ × $\sqrt{3}$)*R*30° and (3 × 3) components) to each reproduce all spectral features observed in the experiment. What is essential is that the combination of features successfully reproduces the experimental spectrum. Therefore, at this point, we can only conclude that a mixture of models C and D is not possible.

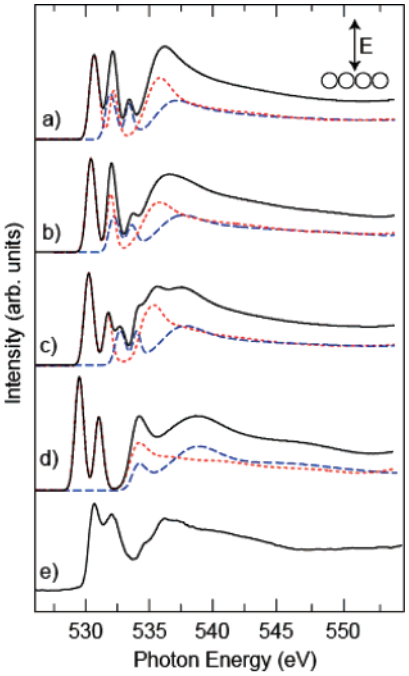

Figure 7. Computed out-of-plane O 1s XAS spectra for water−hydroxyl mixed layer structures compared to experiment: (a) asymmetric (3 × 3) phase with long OH donating H-bond and short OH accepting H-bonds (model A), (b) asymmetric ($\sqrt{3}$ × $\sqrt{3}$)*R*30° phase with long OH donating H-bond and short OH accepting H-bonds (model B), (c) symmetric ($\sqrt{3}$ × $\sqrt{3}$)*R*30° phase (model C), (d) asymmetric (3 × 3) with short OH donating and long OH accepting H-bonds (model D), and (e) experiment. The dotted and dashed lines are the OH and the H_2O contributions, respectively.

Although model A contains a mixture of both OH and H_2O intensities in the second peak, the ratio of the peak heights is too close to unity to fit the experiment. Model B, on the other hand, shows a similar intensity ratio as in the experiment but slightly overestimates the energy separation between the first and second peak. Model C also reproduces the overall spectral shape of the experiment, particularly the resonance at 534.6 eV, but the intensity ratio between the first and second peak is too large. Model D likewise shows a large intensity ratio between the first and second peak and in addition has a mismatch in energy position of the first peak by about −1 eV compared to the experiment. Furthermore, the spectrum of model D has an intensity dip close to 536 eV, which is not observed in the experimental spectrum. Figure 7 reveals that a mixture of at least two model structures is necessary to reproduce the experimental XAS spectrum, which is not surprising since the LEED pattern indicates that a mixture of structures is present in the stable phase.

To confirm the conclusions reached from LEED and XAS, i.e., that a mixture of structures is necessary, and to further refine the picture of which models compare well with experiment we computed XPS binding energies for OH and H_2O in the various structures. Figure 8 compares experimental and theoretical XPS peaks for the four models. The too large computed binding energy shift between OH and H_2O on Pt(111) in model D (3.89 eV) compared to experiment (1.5 eV) eliminates it from consideration as a plausible structural model. Model C also shows a larger computed binding energy shift between OH and H_2O (2.18 eV) compared to experiment. Due to the width of the experimental XPS spectrum, however, this shift is not so

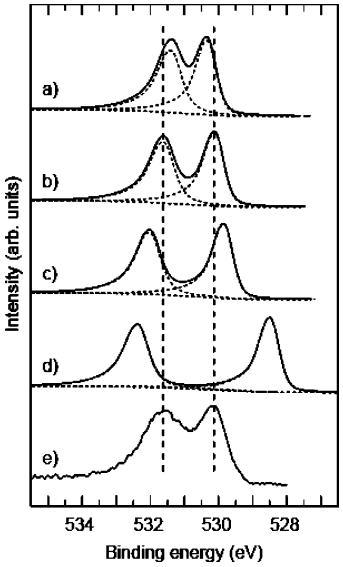

Figure 8. Computed O 1s XPS spectra for water−hydroxyl mixed layer structures compared to the experimental recorded spectrum: (a) asymmetric (3 × 3) phase with long OH donating H-bond and short OH accepting H-bonds (model A), (b) asymmetric ($\sqrt{3} \times \sqrt{3}$)*R*30° phase with long OH donating H-bond and short OH accepting H-bonds (model B), (c) symmetric ($\sqrt{3} \times \sqrt{3}$)*R*30° phase (model C), (d) asymmetric (3 × 3) with short OH donating and long OH accepting H-bonds (model D), and (e) experiment. H_2O and OH components of the computed spectra are shown as dashed lines. The component(s) at lowest binding energy in all spectra (a−e) is that of OH.

large as to conclusively exclude the possibility of a contribution from model C in a mixed phase structure. In contrast, model A has too small a binding energy shift (1.07 eV) compared to experiment (1.5 eV). Model B, on the other hand, shows a binding energy shift (1.52 eV) quite similar to what is found in the experimental XPS spectrum. From an inspection of the experimental spectrum we observe more intensity between the two peaks in comparison with the spectrum of model B. This can be explained as a contribution from structures corresponding to model A, consistent with a mixed ($\sqrt{3} \times \sqrt{3}$)*R*30° and (3 × 3) structure. The large binding energy shift in model C could likewise be combined with contributions from the narrow splitting in model A to offer a reasonable fit with the experiment, as could the XAS spectral features for these two models. Such combinations are considered in Figure 9, which shows the sum of model A with model B (solid) or with model C (dashed) in ($\sqrt{3} \times \sqrt{3}$)*R*30°/(3 × 3) ratios of 1:3, 1:1, and 3:1. The computed mixture that compares most favorably with the XAS data tends to suffer in its agreement with the corresponding XPS data and vice versa. Due to this it is difficult to unambiguously confirm either model as a precise representation of the ($\sqrt{3} \times \sqrt{3}$)*R*30° portion of the mixed phase.

Thus, on the basis of AES and comparing calculated XPS and XAS with experiments, model A, derived from our first-principles DFT calculations, emerges as the most likely structure responsible for the (3 × 3) phase; model D is ruled out by the poor agreement with experiment. For the ($\sqrt{3} \times \sqrt{3}$)*R*30° structure, however, the case is not as clear as both models B and C are in good overall agreement with experimental spectroscopic observations. We could imagine that the best representation of the ($\sqrt{3} \times \sqrt{3}$)*R*30° is in fact a structure with an OH−H_2O bond length somewhere in between that of models B and C; that is, a weakly asymmetric adlayer. Still, it is noteworthy that the asymmetry of model B is accompanied by a variation in O−Pt bond length for OH (2.0−2.1 Å) and H_2O (2.1−2.2 Å). This poses the question of how large a range in

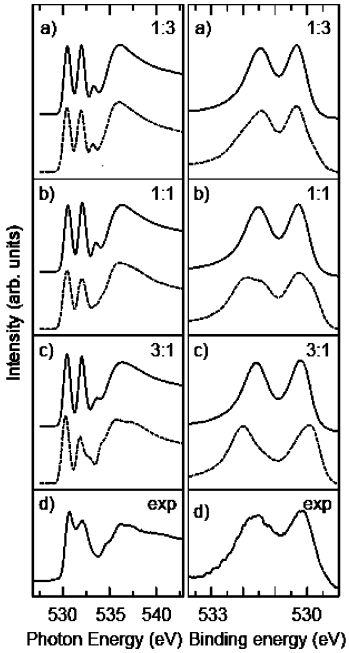

Figure 9. Computed XAS (left panel) and XPS (right panel) spectra for model A summed with model B (solid) and model C (dashed), respectively, representing ($\sqrt{3} \times \sqrt{3}$)*R*30°/(3 × 3) ratios of (a) 1:3, (b) 1:1, and (c) 3:1 compared with (d) experiment.

O−O and O−Pt distances the system can tolerate before the periodicity of the ($\sqrt{3} \times \sqrt{3}$)*R*30° LEED pattern is broken.

4.7. Chemical Driving Force for Stable Bonding. What is the driving force behind the long OH donating and short OH accepting H-bond asymmetry in the models (A and B) predicted by first-principles DFT calculations? The nature of the H-bond in a system of H_2O and OH is primarily electrostatic.[62] To shed light on the details of the chemical bonding that drives the stability of the H-bond structure in the H_2O + OH mixed layer on Pt(111) we turn to XES calculations. Whereas XAS probes unoccupied orbitals, O 1s XES offers a symmetry-selective probe of the occupied p-density of states locally around the oxygen atoms; calculated XES spectra thus provide a population analysis of the wave function closely related to experiment. Comparison of the electron population in the O lp orbital of OH and H_2O in different chemical environments through XES spectrum calculations, separated into p_x-, p_y-, and p_z-components, provides the necessary insight into the details of the H-bonding in the H_2O + OH system on Pt(111). We will in the following discussion focus on the p_z since it corresponds to lone pair orbitals that are of pure p-character oriented in the direction toward the substrate.

Figure 10 shows the computed XES, without dynamical effects,[63] for an isolated H_2O monomer, O−Pt bonding H_2O in the pure water layer on Pt, adsorbed H_2O in the H_2O + OH mixed layer on Pt (taken from model A), OH^- in solution, and adsorbed OH in the H_2O + OH mixed layer on Pt (taken from model A). The O lp occupation (p_z-component) for each case, normalized to the 2.0 p_z electrons for the isolated water monomer, is also given. The differences in integrated intensity of the XES spectra show dramatic rearrangements in the O lp occupation depending on chemical environment. We note a much larger depopulation of the O lp for O−Pt bonding H_2O adsorbed in the H_2O + OH mixed layer ($\Delta p_z = -0.28$ e^-) than for O−Pt bonding H_2O in the pure water layer ($\Delta p_z = -0.07$ e^-). The much higher loss of O lp electron occupation for H_2O in the H_2O + OH mixed layer is mostly related to the fact that

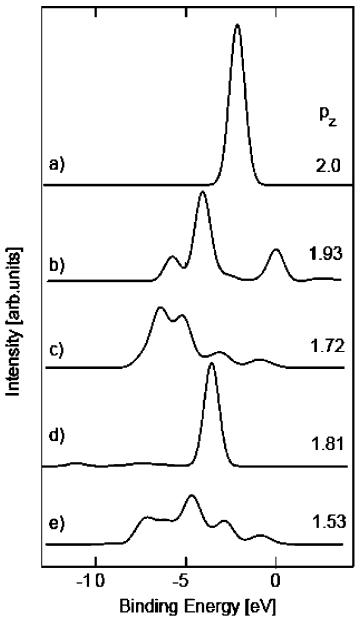

Figure 10. Out-of-plane O 1s XES for (a) water monomer, (b) H_2O/Pt(111), (c) H_2O coadsorbed with OH on Pt(111) (model A), (d) OH^- in solution, and (e) OH coadsorbed with H_2O on Pt(111) (model A). The numerical 2p orbital populations are normalized to O $2p_z = 2$ electrons for the water monomer (a); p_z corresponds to the O lp in each case.

it sits on the order of 0.15 Å closer to the Pt substrate compared to O−Pt bonding H_2O in the pure water layer (2.20 vs 2.35 Å[20]) to facilitate formation of a stable H-bond network. Therefore, to lower the comparatively higher Pauli repulsion for H_2O in the H_2O + OH mixed layer, more O lp electron density has to be polarized away from the region between Pt and O in H_2O; this is accomplished by O lp charge depopulation into the unoccupied Pt d-states. The result is a formal positive charge on H_2O, which is partly distributed to the hydrogen atoms. Consequently, water is a stronger H-bond donor (weaker H-bond acceptor) in the mixed phase compared to pure water on Pt.

In contrast, the near closed-shell electronic structure of OH adsorbed on Pt or in solution leads to a formal negative charge. In solution OH^- is strongly negative which makes it a strong H-bond acceptor. Some of the negative charge spills over to the hydrogen, which makes OH^- a weak H-bond donor. The asymmetry found in the (3 × 3) phase of H_2O + OH on Pt(111), with accepting and donating H-bonds of 2.66 and 3.16 Å, respectively, is comparable to OH^- in solution[39] and is primarily driven by the strong H_2O (donor)−OH (acceptor) bond. Differences, although small, in bonding between the two systems are reflected in the significantly lower O lp occupation for adsorbed OH ($p_z = 1.53$) compared to OH^- in solution ($p_z = 1.81$), shown in Figure 10. The Pt surface has a significant influence on the charge rearrangement, manifested here in two ways. First, the depopulation of charge into Pt orbitals reduces the degree of charge spillover to the H. This is expressed in the lower O lp population for OH on Pt compared to solution. Second, there is an additional contraction of charge along the O−H bond (p_y-component; not shown in Figure 10) away from the hydrogen so that more charge is concentrated on the oxygen ($p_y = 1.85$) for OH adsorbed on Pt compared to OH^- in solution ($p_y = 1.39$). Hence, OH on Pt is a slightly stronger donor of H-bonds than it is in solution. This, combined with the pinning of the overlayer to the registry of the Pt substrate, can account for the less pronounced asymmetry in the (3 × 3) phase of H_2O + OH on Pt(111) compared to solution. The specific asymmetry of the H_2O + OH mixed layer on Pt(111) can therefore be attributed to a cooperativity effect between H-bonding in the overlayer and interaction with the substrate.

5. Conclusions

XPS, XAS, AES, and LEED along with first-principles DFT-based electronic structure calculations and XPS/XAS spectrum calculations have shown that hydroxyl and water coadsorbed on Pt(111), formed by exposing a (2 × 2)-O precovered surface to a saturating amount of D_2O, consists of two hexagonal structures: $(\sqrt{3} \times \sqrt{3})R30°$ and (3 × 3). The results are in agreement with earlier studies by Bedürftig et al.,[3] Clay et al.,[4] and Held et al.[19] In addition, XPS, AES, and XAS measurements come together with total energy and XES calculations to indicate that both the $(\sqrt{3} \times \sqrt{3})R30°$ and (3 × 3) structures most likely have asymmetric H-bond lengths where the OH donating H-bonds are long and the OH accepting H-bonds are short. XAS also reveals that the H-bond network parallel to the Pt surface is saturated and includes both hydroxyl and water lying flat with only oxygen bonded to the Pt atoms, which is consistent with earlier DFT-based calculations[1,2,15−17] and an IR study.[4] Both H_2O and OH occupy top sites with H_2O−Pt and HO−Pt distances of 2.20 and 2.10 Å, respectively, closer to Pt than in the corresponding pure water case (∼2.35 Å[20]). Temperature-dependent XPS shows that D_2O + OD on Pt(111) is more stable than the corresponding pure D_2O case and thereby supports TPD studies reporting a higher water desorption temperature compared to the corresponding pure water case.[4,14] XES calculations elucidate how the H-bonding network is modified due to interaction with the Pt substrate and the mechanism by which water is a stronger donor in the mixed phase compared to pure water on Pt.

Acknowledgment. This work was supported by the Division of Material Sciences and Engineering, Office of Basic Energy Sciences, U.S. Department of Energy under the auspices of the President's Hydrogen Fuel Initiative, the Swedish Foundation for Strategic Research, and the Swedish Natural Science Research Council. The Advanced Light Source is supported by the Director, Office of Science, Office of Basic Energy Sciences, Material Sciences Division, of the U.S. Department of Energy under Contract No. DE-AC03-76SF00098 at Lawrence Berkeley National Laboratory. This research was mainly carried out at the Stanford Synchrotron Radiation Laboratory, a national user facility operated by Stanford University on behalf of the U.S. Department of Energy, Office of Basic Energy Sciences. Generous grants of computer time at the Swedish National Supercomputer Center and the Center for Parallel Computing, Sweden, are gratefully acknowledged.

References and Notes

(1) Michaelides, A.; Hu, P. *J. Chem. Phys.* **2001**, *114*, 513.
(2) Michaelides, A.; Hu, P. *J. Am. Chem. Soc.* **2001**, *123*, 4235.
(3) Bedürftig, K.; Völkening, S.; Wang, Y.; Wintterlin, J.; Jacobi, K.; Ertl, G. *J. Chem. Phys.* **1999**, *111*, 11147.
(4) Clay, C.; Haq, S.; Hodgson, A. *Phys. Rev. Lett.* **2004**, *92*, 046102.
(5) Völkening, S.; Bedürftig, K.; Jacobi, K.; Wintterlin, J.; Ertl, G. *Phys. Rev. Lett.* **1999**, *83*, 2672.
(6) Creighton, J. R.; White, J. M. *Surf. Sci.* **1982**, *122*, L648.
(7) Bange, K.; Madey, T. E.; Sass, J. K.; Stuve, J. M. *Surf. Sci.* **1987**, *183*, 334.
(8) Fisher, G. B.; Sexton, B. A.; Gland, J. L. *J. Vac. Sci. Technol.* **1980**, *17*, 144.
(9) Gland, J. L. *Surf. Sci.* **1980**, *93*, 487.
(10) Steininger, H.; Lehwald, S.; Ibach, H. *Surf. Sci.* **1982**, *123*, 1.
(11) Mortensen, K.; Klink, C.; Jensen, F.; Besenbacher, F.; Stensgaard, I. *Surf. Sci.* **1989**, *220*, L701.

(12) Björneholm, O.; Nilsson, A.; Tillborg, H.; Bennich, P.; Sandell, A.; Hernäs, B.; Puglia, C.; Mårtensson, N. *Surf. Sci.* **1994**, *315*, L983.
(13) Fisher, G. B.; Gland, J. L. *Surf. Sci.* **1980**, *94*, 446.
(14) Fisher, G. B.; Sexton, B. A. *Phys. Rev. Lett.* **1980**, *44*, 683.
(15) Karlberg, G. S.; Olsson, F. E.; Persson, M.; Wahnström, G. *J. Chem. Phys.* **2003**, *119*, 4865.
(16) Karlberg, G. S.; Wahnström, G. *Phys. Rev.* **2004**, *92*, 136103.
(17) Karlberg, G. S.; Wahnström, G. *J. Chem. Phys.* **2005**, *122*, 194705.
(18) Seitsonen, A. P.; Zhu, Y.; Bedürftig, K.; Over, H. *J. Am. Chem. Soc.* **2001**, *123*, 7347.
(19) Held, G.; Clay, C.; Barrett, S. D.; Haq, S.; Hodgson, A. *J. Chem. Phys.* **2005**, *123*, 064711.
(20) Ogasawara, H.; Brena, B.; Nordlund, D.; Nyberg, M.; Pelmenschikov, A.; Pettersson, L. G. M.; Nilsson, A. *Phys. Rev. Lett.* **2002**, *89*, 276102-1.
(21) Nilsson, A. *J. Electron Spectrosc. Relat. Phenom.* **2002**, *126*, 3.
(22) Wernet, Ph.; Nordlund, D.; Bergmann, U.; Cavalleri, M.; Odelius, M.; Ogasawara, H.; Näslund, L.-Å.; Hirsch, T. K.; Ojamäe, L.; Glatzel, P.; Pettersson, L. G. M.; Nilsson, A. *Science* **2004**, *304*, 995.
(23) Cavalleri, M.; Ogasawara, H.; Pettersson, L. G. M.; Nilsson, A. *Chem. Phys. Lett.* **2002**, *364*, 363.
(24) Cavalleri, M.; Nordlund, D.; Odelius, M.; Nilsson, A.; Pettersson, L. G. M. *Phys. Chem. Chem. Phys.* **2005**, *7*, 2854.
(25) Odelius, M.; Cavalleri, M.; Nilsson, A.; Pettersson, L. G. M. *Phys. Rev. B* **2006**, *73*, 024205.
(26) Sandell, A.; Björneholm, O.; Nilsson, A.; Zdansky, E. O.; Tillborg, H.; Andersen, J. N.; Mårtensson, N. *Phys. Rev. Lett.* **1993**, *70*, 2000.
(27) Sandell, A.; Björneholm, O.; Nilsson, A.; Hernnäs, B.; Andersen, J. N.; Mårtensson, N. *Phys. Rev. B* **1994**, *49*, 10136.
(28) Öström, H.; Ogasawara, H.; Näslund, L.-Å.; Pettersson, L. G. M.; Nilsson, A. *Phys. Rev. Lett.* **2006**, *96*, 146104.
(29) Schiros, T.; Haq, S.; Ogasawara, H.; Takahashi, O.; Öström, H.; Andersson, K.; Pettersson, L. G. M.; Hodgson, A.; Nilsson, A. *Chem. Phys. Lett.* **2006**, *429*, 415.
(30) VG Scienta AB. http://www.vgscienta.com, May 7, 2002.
(31) Stöhr, J. *NEXAFS Spectroscopy*; Springer-Verlag: New York, 1992.
(32) SPECS Scientific Instruments, Inc. http://www.specs.com, June 2, 2003.
(33) Goodfellow Corp. http://www.goodfellow.com, July 29, 2002.
(34) Jo, S. K.; Kiss, J.; Polanco, J. A.; White, J. M. *Surf. Sci.* **1991**, *253*, 233.
(35) Gland, J. L.; Sexton, B. A.; Fisher, G. B. *Surf. Sci.* **1980**, *95*, 587.
(36) Andersson, K.; Gómez, A.; Glover, C.; Nordlund, D.; Öström, H.; Schiros, T.; Takahashi, O.; Ogasawara, H.; Pettersson, L. G. M.; Nilsson, A. *Surf. Sci.* **2005**, *585*, L183.
(37) Steininger, H.; Lehwald, S.; Ibach, H. *Surf. Sci.* **1982**, *123*, 264.
(38) Perdew, J. P.; Chevary, J. A.; Vosko, S. H.; Jackson, K. A.; Pederson, M. R.; Singh, D. J.; Fiolhais, C. *Phys. Rev. B* **1992**, *46*, 6671.
(39) Botti, A.; Bruni, F.; Imberti, S.; Ricci, M. A.; Soper, A. K. *J. Chem. Phys.* **2004**, *120*, 10154.
(40) Gropen, O.; Almloef, J.; Wahlgren, U. *NATO ASI Ser., Ser. B (Cluster Models Surf. Bulk Phenom.)* **1992**, *283*, 453.
(41) Huzinaga, S. *J. Chem. Phys.* **1965**, *42*, 1293.
(42) Kutzelnigg, W.; Fleischer, U.; Schindler, M. *NMR—Basic Principles and Progress*; Springer-Verlag: Heidelberg, Germany, 1990.
(43) Pettersson, L. G. M.; Wahlgren, U.; Gropen, O. *J. Chem. Phys.* **1987**, *86*, 2176.
(44) Hermann, K.; Pettersson, L. G. M.; Casida, M. E.; Daul, C.; Goursot, A.; Koester, A.; Proynov, E.; St-Amant, A.; Salahub, D. R.; Carravetta, V.; Duarte, A.; Godbout, N.; Guan, J.; Jamorski, C.; Leboeuf, M.; Malkin, V.; Malkina, O.; Nyberg, M.; Pedocchi, L.; Sim, F.; Triguero, L.; Vela, A. STOBE Software, 2002.
(45) Becke, D. *Phys. Rev. A* **1988**, *38*, 3098.
(46) Perdew, J. P. *Phys. Rev. B* **1986**, *33*, 8822.
(47) Triguero, L.; Pettersson, L. G. M.; Ågren, H. *Phys. Rev. B* **1998**, *58*, 8097.
(48) Ågren, H.; Carravetta, V.; Vahtras, O.; Pettersson, L. G. M. *Theor. Chem. Acc.* **1997**, *97*, 14.
(49) Kolczewski, C.; Püttner, R.; Plashkevych, O.; Ågren, H.; Staemmler, V.; Martins, M.; Snell, G.; Sant'anna, M.; Kaindl, G.; Pettersson, L. G. M. *J. Chem. Phys.* **2001**, *115*, 6426.
(50) Takahashi, O.; Pettersson, L. G. M. *J. Chem. Phys.* **2004**, *121*, 10339.
(51) Nordlund, D.; Ogasawara, H.; Wernet, Ph.; Nyberg, M.; Odelius, M.; Pettersson, L. G. M.; Nilsson, A. *Chem. Phys. Lett.* **2004**, *395*, 161.
(52) Triguero, L.; Plashkevytch, O.; Pettersson, L. G. M.; Ågren, H. *J. Electron Spectrosc. Relat. Phenom.* **1999**, *104*, 195.
(53) Föhlisch, A.; Hasselström, J.; Bennich, P.; Wassdahl, N.; Karis, O.; Nilsson, A.; Triguero, L.; Nyberg, M.; Pettersson, L. G. M. *Phys. Rev. B* **2000**, *61*, 16229.
(54) Puglia, C.; Nilsson, A.; Hernnäs, B.; Karis, O.; Bennich, P.; Mårtensson, N. *Surf. Sci.* **1995**, *342*, 119.
(55) Michaelides, A.; Ranea, V. A.; de Andres, P. L.; King, D. A. *Phys. Rev. Lett.* **2003**, *90*, 216102.
(56) Andersson, K.; Nikitin, A.; Pettersson, L. G. M.; Nilsson, A.; Ogasawara, H. *Phys. Rev. Lett.* **2004**, *93*, 196101.
(57) Denzler, D. N.; Hess, C.; Dudek, R.; Wagner, S.; Frischkorn, C.; Wolf, M.; Ertl, G. *Chem. Phys. Lett.* **2003**, *376*, 618.
(58) Beniya, A.; Yamamoto, S.; Mukai, K.; Yamashita, Y.; Yoshinobu, J. *J. Chem. Phys.* **2006**, *125*, 054717.
(59) Hermann, K.; Witko, M.; Pettersson, L. G. M.; Siegbahn, P. *J. Chem. Phys.* **1993**, *99*, 610.
(60) Patrito, E. M.; Paredes-Olivera, P. *Surf. Sci.* **2003**, *527*, 149.
(61) Myneni, S.; Luo, Y.; Näslund, L-Å.; Cavalleri, M.; Ojamäe, L.; Ogasawara, H.; Pelmenschikov, A.; Wernet, Ph.; Väterlein, P.; Heske, C.; Hussain, Z.; Pettersson, L. G. M.; Nilsson, A. *J. Phys.: Condens. Matter* **2002**, *14*, L213.
(62) Jeffrey, G. A. *An Introduction to Hydrogen Bonding*; Oxford University Press: Oxford, 1997.
(63) Brena, B.; Nordlund, D.; Odelius, M; Ogasawara, H.; Nilsson, A.; Pettersson, L. G. M. *Phys. Rev. Lett.* **2004**, *93*, 148302.